CERN, 23 October 2001

# μ–LANNDD

## A prototype magnetized liquid Argon detector for electron charge sign discrimination

## PROPOSAL

*Franco Sergiampietri*

*INFN-UCLA-HAWAII-PRINCETON-ETH-CERN Collaboration*

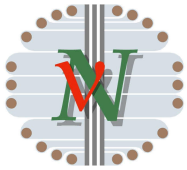

**Abstract**

A liquid Argon TPC detector immersed in magnetic field is proposed for systematic study and parameter optimisation in electron/muon charge sign discrimination and muon momentum determination by magnetic deflection. Design criteria and preliminary calculation are described.

**Table of content**

Introduction ..... 5
1. Event simulation ..... 7
2. The magnet ..... 8
2.1. TPC in magnetic field ..... 8
2.2. Charge sign discrimination ..... 9
2.3. Measurement of muon momenta ..... 10
2.4. Construction ..... 10
3. The liquid Argon TPC ..... 11
3.1. Configuration ..... 11
3.2. Wire chamber ..... 12
3.3. Electronics ..... 13
4. The cryostat ..... 14
4.1. Heat input, insulation and LN2 consumption ..... 14
5. Cryogenic set-up ..... 15
6. The test beam set-up ..... 15
Appendix. Time schedule, cost estimate, collaboration ..... 16

## Introduction

A detector with an active mass of 70 *kTon*, based on the liquid Argon TPC technique and immersed in magnetic field is under study and its final proposal is under preparation[1],[2]. The detector, named LANNDD (Figure 1), is planned to be situated underground. The site considered at present is CUNL (Carlsbad UNderground Laboratory, New Mexico). The main physics program inspiring this project concerns the nucleon decay physics and the physics of neutrino oscillations with long base line beams from possible neutrino factories at present under study in the United States, in Japan and at CERN. The main lines and the work made on this project have been recently described in a contribution at the NuFACT'01 workshop.

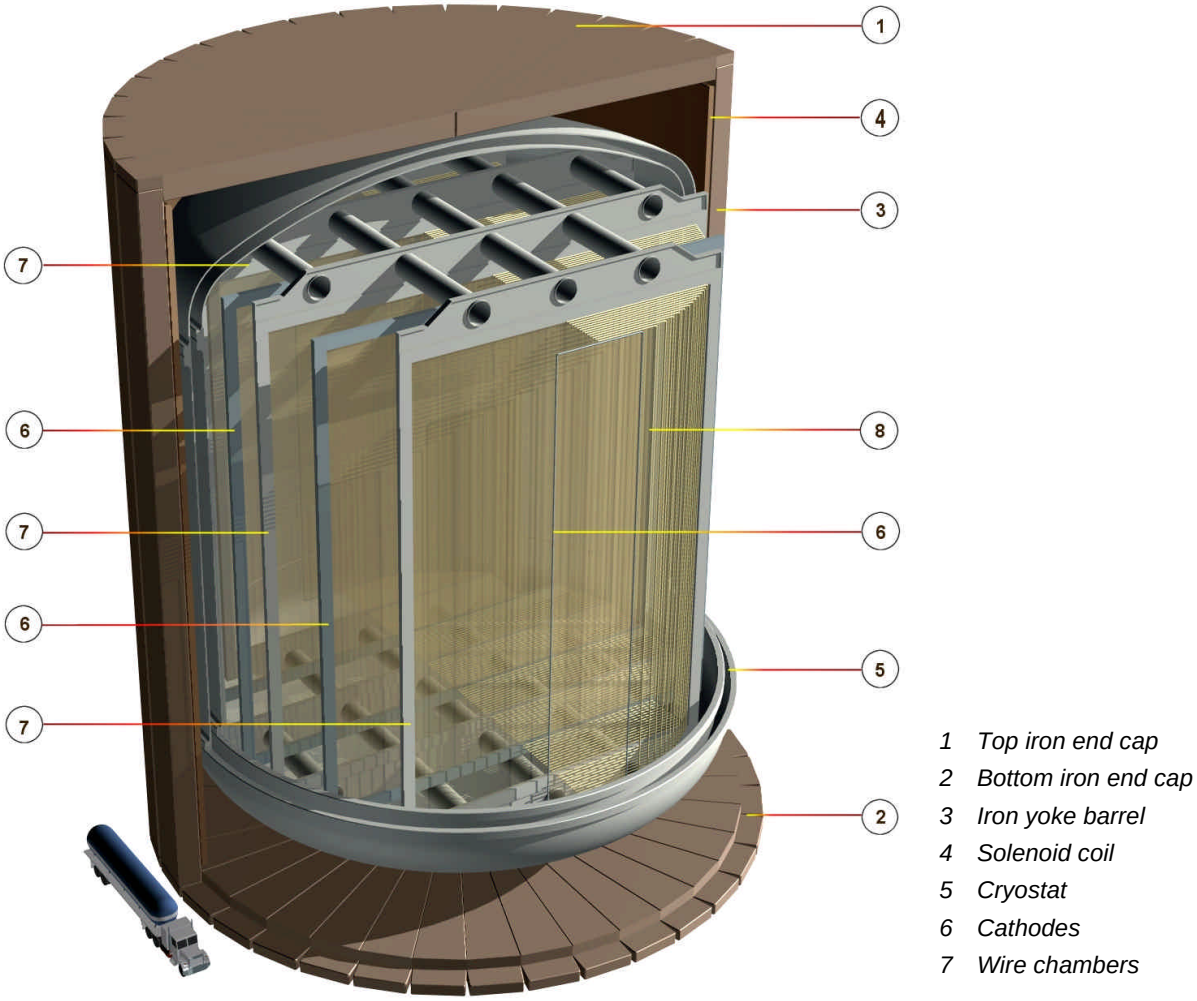


**Figure 1:** Cutaway view of the LANNDD detector.

Due to its specific measuring potentialities (see for example the event in Figure 2), as fine-grain 3d-imaging, *dE/dx* tracking, hadron/electromagnetic calorimetric response, the liquid Argon TPC appears to be an ideal instrument for detection and reconstruction of neutrino interaction events. While on the liquid Argon TPC technique a remarkable experience has been accumulated[3], other features of the LANNDD

---

[1] D. B. Cline, J. G. Learned, K. McDonald and F. Sergiampietri, *LANNDD – A Massive Liquid Argon Detector for Proton Decay, Supernova and Solar Neutrino Studies, and a Neutrino Factory Detector*. Proceedings of the NuFACT'01 Workshop, Tsukuba, Ibaraki, Japan, May 24-30, 2001; Astro-PH/0105442.

[2] D. B. Cline and F. Sergiampietri, *A Super Beam to the LANNDD Detector at the Carlsbad Underground Laboratory*. Contribution to the Snowmass 2001 Workshop.

[3] ICARUS detector: for a description and a complete reference list visit the sites http://www.aquila.infn.it:80/icarus/index.html and http://pcnometh4.cern.ch.

project, related mainly to the imaging in magnetic field and to the operation in extremely large volume sizes, need a dedicated R&D (see ref. 1).

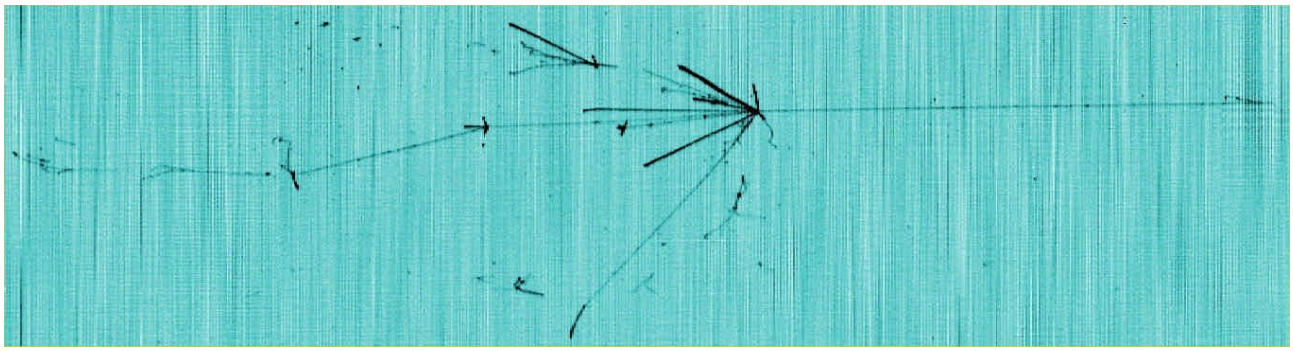

**Figure 2:** Nuclear interaction recorded in ICARUS T600 during the first setting-up of the detector.

In the case of neutrino beams from neutrino factories based on muon storage rings, the detection of CC-neutrino interactions with ($e$, μ) leptons with charge sign opposite to that expected from the stored μ sign, is, by itself, a proof of oscillation. The identification of the charge sign for $e$ and μ, through magnetic deflection comes out to be the qualifying feature of detectors for this physics. While for muons, given the long detectable path in detectors of the considered size, deflections are rather easily detectable against the multiple scattering even at field intensities of ~0.2 $T$, for electrons the useful tracking is only the path of the primary $e^{\pm}$ before showering (1÷2 $X_o$) and the required magnetic field intensity should range over ~0.5 $T$. From simulations, it results that, in many cases, the electromagnetic shower axis follows, along several radiation lengths, the path of the primary electron and then the shower appears bent accordantly with the sign and the momentum of the primary electron.

The electron charge sign identification results then an interesting and intriguing theme to be worked up with a dedicated R&D program. The program is based on a liquid Argon TPC to be tested in a 1÷4 *GeV/c* electron test beam. The active volume should have good shower containment (~15$X_o$ length, 4$R_M$ transverse size). The cryostat is outfitted with a solenoid coil able to generate fields up to ~1T.

With such a device it will be possible also a systematic study of the operating parameters in the muon momentum measurement by magnetic deflection in a liquid Argon TPC.

## 1. Event simulation

Results of a Montecarlo simulation on electromagnetic showers in a liquid Argon TPC immersed in magnetic field have been shown at the NuFACT'01 Workshop[4].

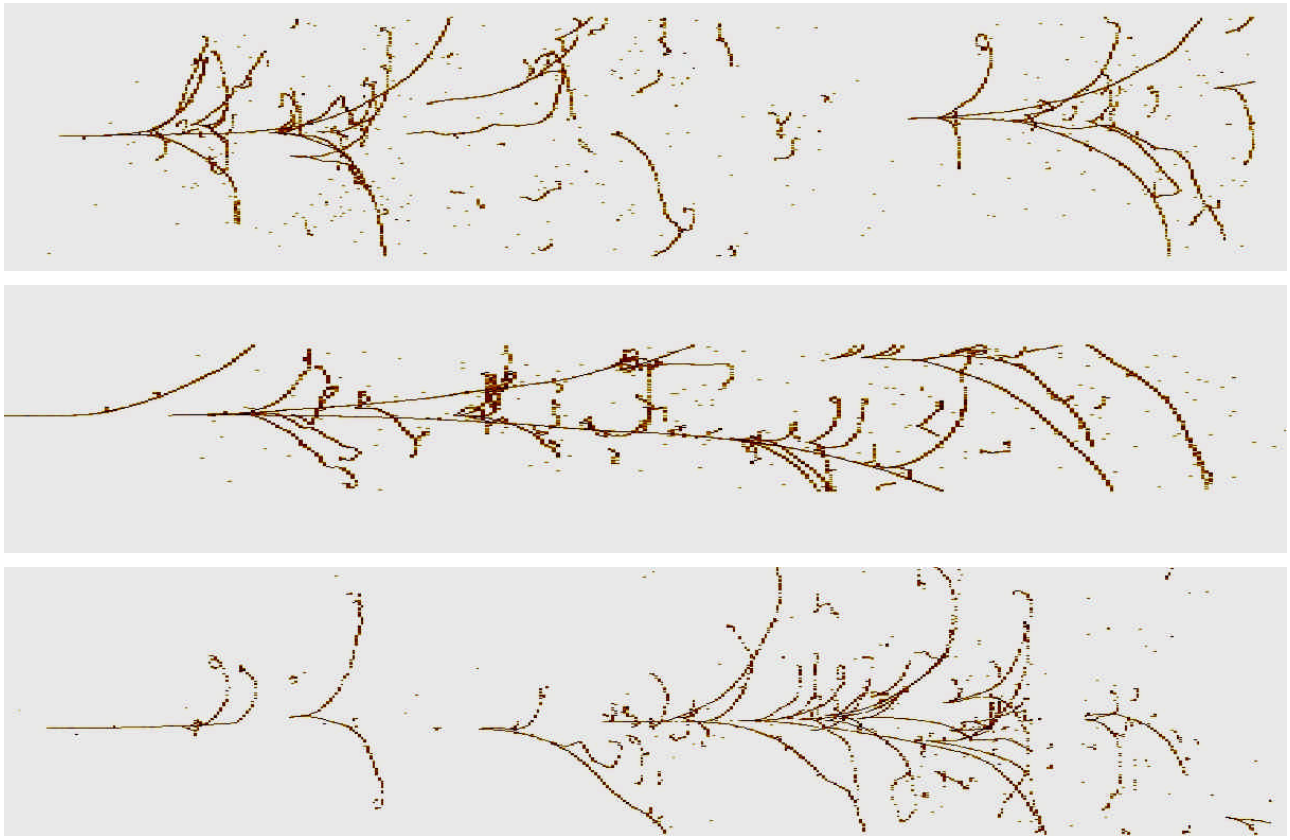

**Figure 3:** Montecarlo generated electromagnetic showers in a magnetised liquid Argon TPC. $E_{sh}$ = 2.5 *GeV*, $B$ = 1 *T*.

For showers completely contained in the active volume, the calorimetric measure gives the energy and then the curvature radius that, fitted to the initial part of the shower on the left or on the right of its axis, in many cases indicates the sign of the initiating electron.

In most cases, the initial electron continues to be the leading particle for more than one or two radiation length and then we can observe an average bending of the shower (statistical sign discrimination).

When the initial electron emits a high-energy gamma, its momentum and its curvature radius are significantly reduced making easier the sign identification (see, for example, the two lower events in Figure 3).

[4] M. Campanelli, *Study of effects related to the delta-phase (CP/T violation) in neutrino oscillations at a neutrino factory*, Proceedings of the NUFACT'01 WORKSHOP, Tsukuba, Ibaraki, Japan, May 24-30, 2001.

## 2. The magnet

### *2.1. TPC in magnetic field*

In a TPC, the active volume is immersed in an electric field $\vec{E}_d$ to drift the electrons, generated by an ionising particle, towards a wire chamber anode (*time projection*). In a simple configuration the wire chamber is made by two wire planes, with the wires of the first plane aligned in a direction orthogonal to that of the wire of the second plane. With an electric field $\vec{E}_c \cong (1.2 \div 2) \cdot \vec{E}_d$ established between the two wire planes, drifting electrons pass through the first encountered wire plane (*induction* plane), inducing a negative charge signal on it, when approaching, followed by a positive signal when leaving it. Electrons are then collected in the second wire plane (*collection* plane) generating a negative charge signal on the encountered wires. This mechanism generates a second *geometrical projection* along the coordinates associated with the two wire directions.

For charge sign discrimination (and for momentum estimation) a magnetic field $\vec{B}$ should be applied orthogonal or parallel to $\vec{E}_d$.

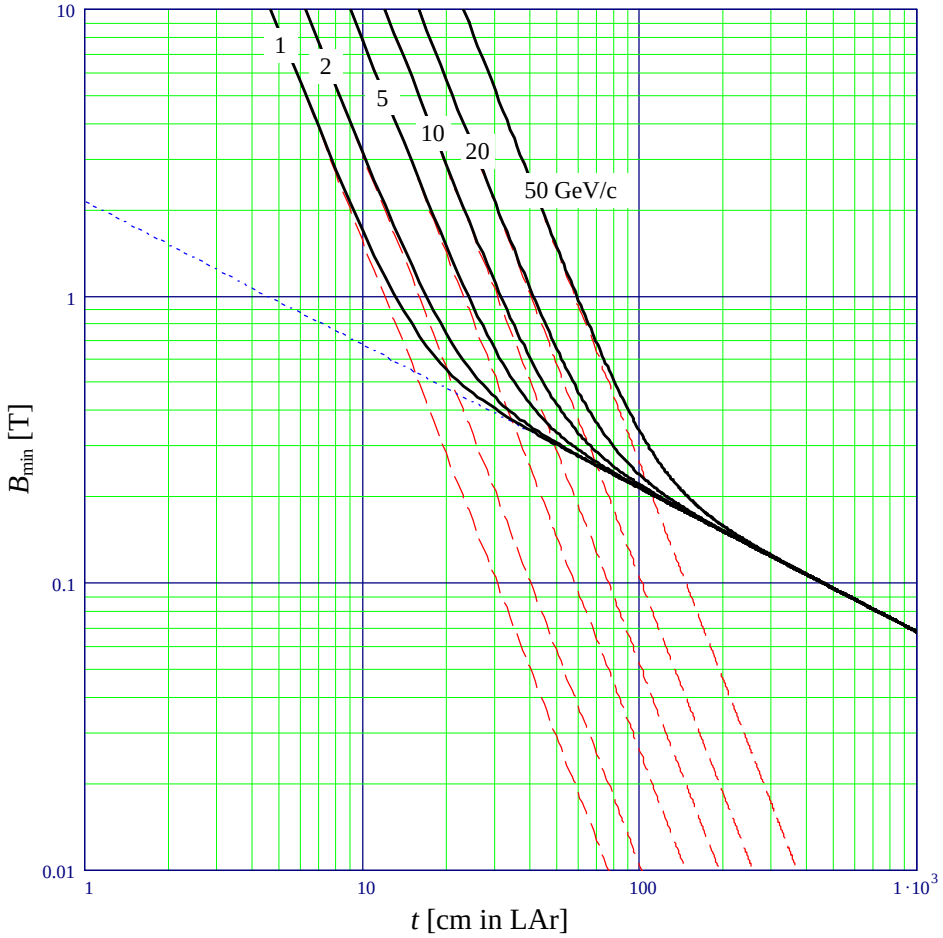


**Figure 4:** Minimum magnetic field satisfying the condition (2) vs. track length. Dashed curves: contribution of the detector resolution at momenta 1, 2, 5, 10, 20 and 50 GeV/c. Dotted curve: contribution of the multiple scattering in the range 1÷50 GeV/c. Solid thick curves: combined contribution of detector resolution and multiple scattering in the range 1÷50 GeV/c.

With $\vec{B} \| \vec{E}_d$, the maximum bending is obtained for tracks originally contained in a plane orthogonal to $\vec{B}$ and then parallel to the wire plane. Their ionisation electrons arrive then at the same time on the wires,

generating degenerate images as straight segments. On the contrary, with $\vec{B} \perp \vec{E}_d$, tracks in the maximum bending plane are imaged as arc of circle (or ellipse) in almost one of the wire planes.

This justifies the choice for the $\vec{B} \perp \vec{E}_d$ configuration.

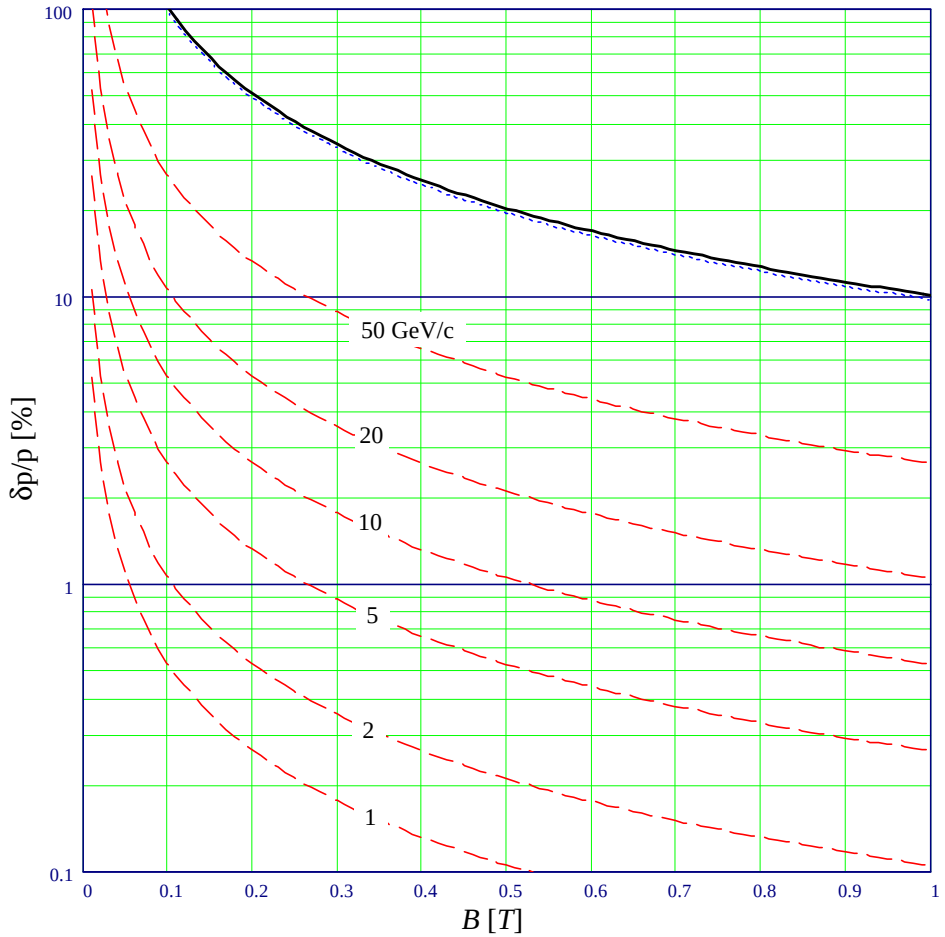


**Figure 5:** Momentum resolution vs. magnetic field for muons crossing 15 $X_o$ in liquid Argon. Dashed curves: contribution of the detector resolution at momenta 1, 2, 5, 10, 20 and 50 *GeV/c*. Dotted curve: contribution of the multiple scattering not depending on momentum. Solid thick curves: combined contribution of detector resolution and multiple scattering in the range 1÷50 *GeV/c*.

### *2.2. Charge sign discrimination*

For charge sign discrimination, the magnetic bending should be stronger then the multiple scattering and distinguishable against the detector resolution. In both cases, we have to discriminate, between positive and negative curvatures.

The dependence on the available track length of the minimum magnetic field intensity required to discriminate the charge sign at 3σ-level is reported in Figure 4. It results that: *a)* for muons with track lengths over one meter, charge sign discrimination is feasible even at momenta greater than 50 *GeV/c*, with $B \geq 0.2$ *T*; *b)* for electrons, assuming $2X_o$ track lengths, detector 3d-pixel size $\Delta = 3.4$ *mm* and $B = 1$ *T*, charge sign discrimination is possible for momenta up to 7.7 *GeV/c*.

To experimentally verify the above results with a prototype detector, magnetic field intensities in the range 0.7÷1.0 *T* should be considered.

### 2.3. *Measurement of muon momenta*

Momentum determination through the measurement of the curvature in magnetic field is a precious tool for the total energy evaluation of CC-neutrino interaction events, with muons escaping the active detector volume.

As for charge sign discrimination, momentum resolution is limited by multiple scattering and detector granularity. Its dependence on the applied magnetic field is reported in Figure 5, showing that for tracks completely crossing the detector length, momentum resolutions of 10% at 1 *T* (20% at 0.5 *T*) are reachable.

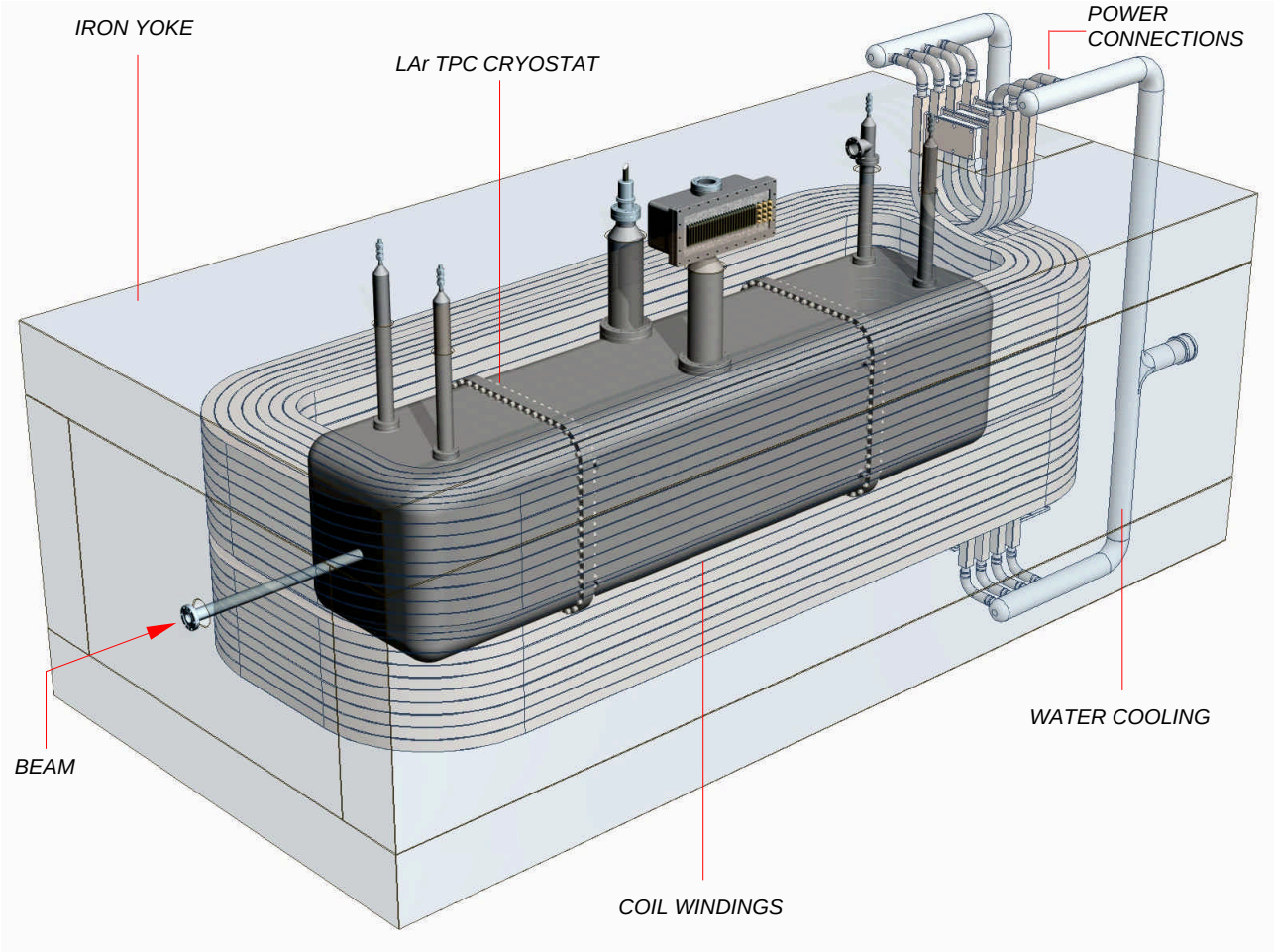


**Figure 6:** View of the detector, outfitted with the magnetic coil and the return iron yoke. The beam entrance evacuated pipe is indicated on the left (front side).

### 2.4. *Construction*

The magnet is configured as a solenoid surrounding the detector. The magnetized volume is defined by:

Height..... $h$ = 614 *mm*
Width..... $w$ = 610 *mm*
Length ..... $l$ = 2300 *mm*

For a magnetic flux intensity $B = 1T$, electrical parameters result as:

Total current..... $I$ = 3.8 *kA*
Total power ..... $W$ = 249 *kW*
Copper mass..... $M_{Cu}$ = 6 *ton.*
Iron yoke mass .....$M_{Fe}$ = 31 *ton*

The full construction is sketched in Figure 6.

## 3. The liquid Argon TPC

The layout of the detector is based on the following choices:

– Square base parallelepiped active volume lying in the horizontal plane, 2112×384×384 $mm^3$ in volume.

– Drift along the horizontal direction, from left to right, perpendicular to the long axis.

– Magnetic field along the vertical direction, perpendicular to the long axis.

With this geometry, beam particle tracks (aligned along the long axis) are bent in a horizontal plane and projected toward a wire chamber in the right vertical plane (see Figure 7).

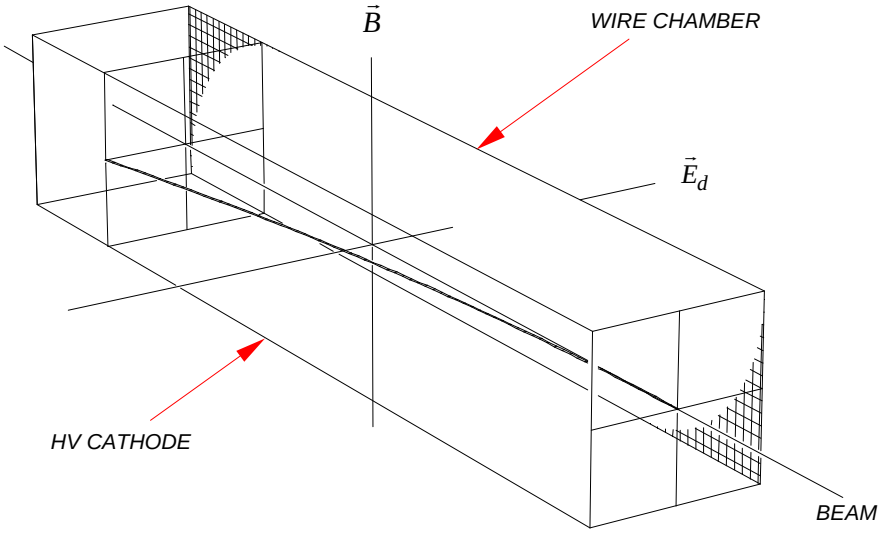


**Figure 7:** Schematic layout of the chamber geometry.

### *3.1. Configuration*

The LAr TPC configuration, shown in Figure 9, is based on a high voltage cathode plane and a two-plane wire chamber aligned on two vertical planes parallel to the beam direction. Wires on the first chamber plane are aligned along the horizontal direction while wires on the second plane are aligned along the vertical direction. Wires are individually connected, through twisted pair cables and through a hermetic multi-contacts feedthrough, to low noise preamplifiers (virtual ground).

A set of equally spaced electrodes (field shaping electrodes), dc-biased at linearly decreasing voltages between the cathode and the ground voltages, surrounds the active volume to maintain the drift field uniform across it. The Figure 8 shows the electric field uniformity inside the active LAr volume.

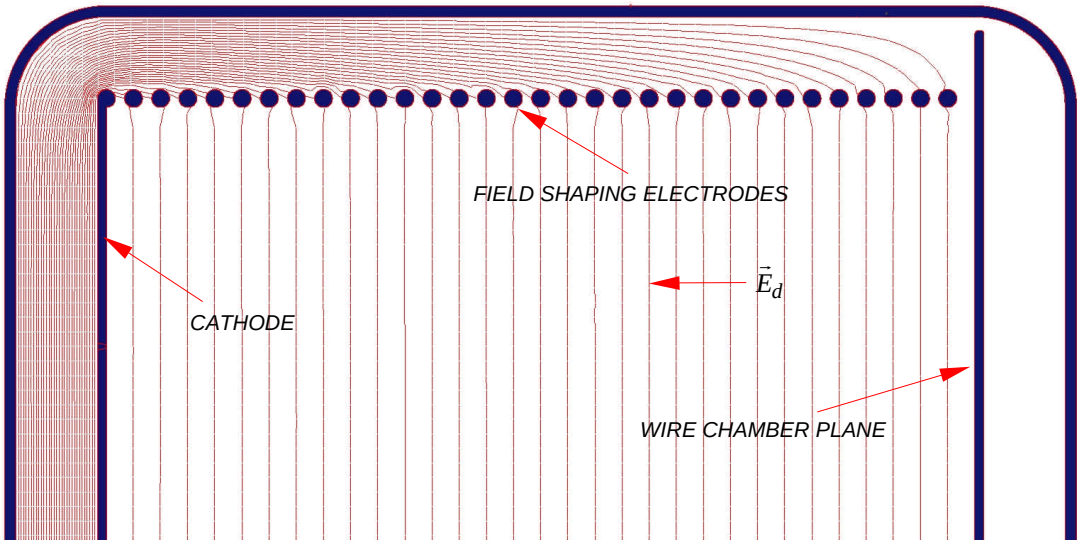


**Figure 8:** Equipotenal lines inside and outside the active LAr volume, in the upper half of the vertical cross-section of the TPC.

### *3.2. Wire chamber*

The main parameters of the wire chamber are summarized in Table 1.

**Table 1:** Wire chamber parameters

| | |
|---|---|
| Number of wire planes | 2 (***I***: Induction wires, ***C***: collection wires) |
| Wire angle with the horizontal direction | |
| Plane ***I***: | 0° |
| Plane ***C***: | 90° |
| Number of wires | 832 |
| Plane ***I***: | 128 |
| Plane ***C***: | 704 |
| Wire diameter | 100 μ*m* (hard drawn stainless steel) |
| Wire pitch | 3 *mm* |
| Wire plane spacing | 4 *mm* |
| Wire DC-bias voltage | |
| Plane ***I***: | 0 *volt* |
| Plane ***C***: | ≤ +400 *volt* (with drift field $E_d$ = 500 *V/cm*) |

The wires are directly soldered to printed circuit boards in groups of 32. At one wire end, the boards are equipped with a 68-pin connector for signal transmission to the front-end electronics via twisted pair cables. Two coaxial connectors are soldered on each of the boards at the other wire ends, for calibration charge injection independently on odd and even wires, through printed circuit capacitors. The printed circuit boards are mechanically fastened to a rigid stainless steel frame (see Figure 9).

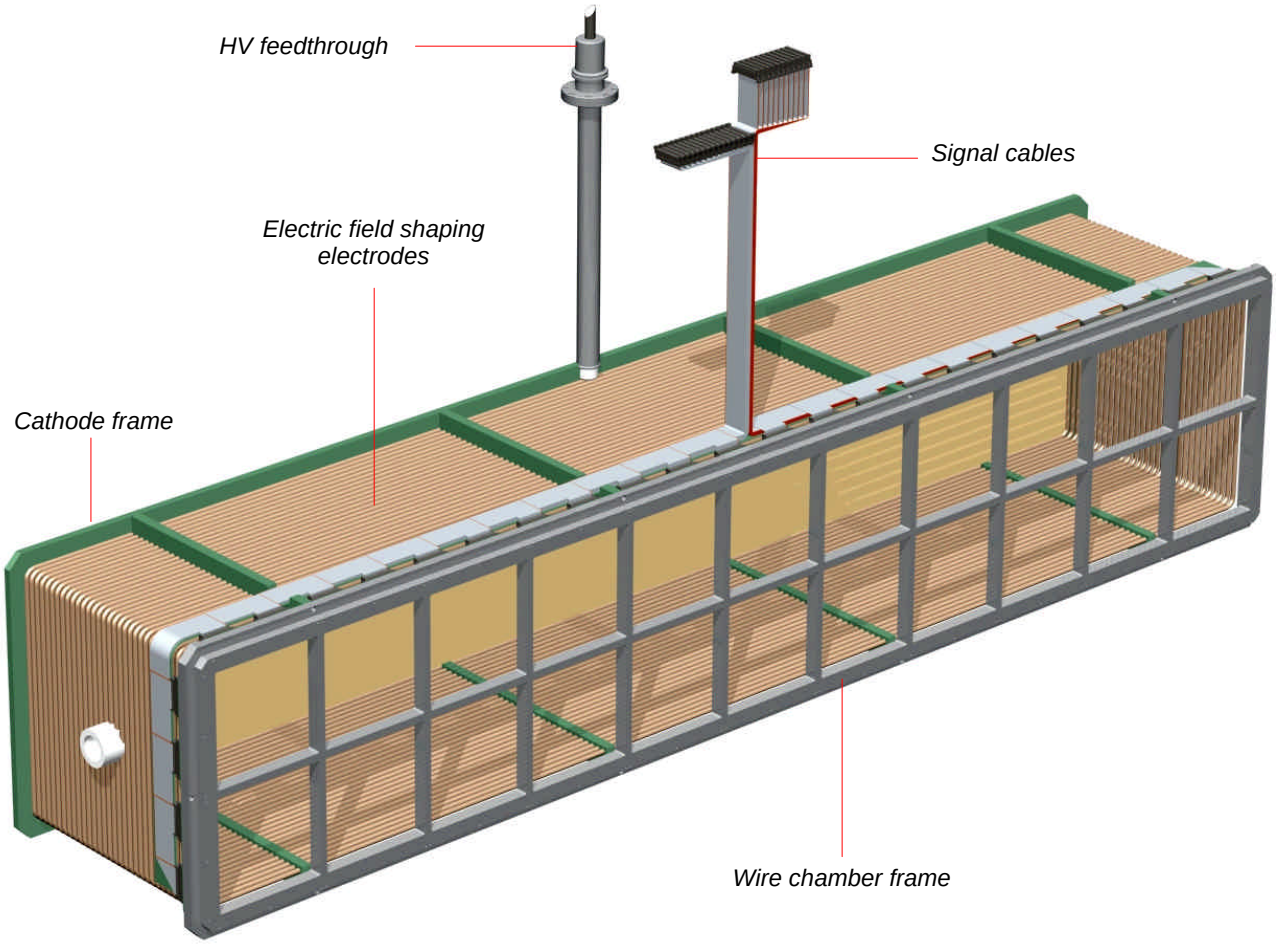


**Figure 9:** Time projection chamber configuration.

### *3.3. Electronics*

Signal cables are connected via the signal feedthrough and individual de-coupling capacitors to low noise preamplifiers. Drifting electrons induce bi-polar current signal on the induction wires (negative sign, when approaching to the wires, followed by a positive sign when leaving the wires towards the collection plane) and uni-polar negative charge sign on the collection wires. Charge preamplifiers are then required at the front-end for the induction wires (current integration on a uni-polar negative charge signal) and current preamplifiers (or charge preamplifiers with short peaking time) for the collection wires. With this solution, the acquired signals are of the same order of amplitude in both planes. After amplification and digital conversion, the signals are memorised in buffer memories and read-out by the computer.

The electronics for the read-out of the ICARUS[3] detector is designed on this principle and it will be used for this test as first solution, by actually adapting the shaping and amplification parameters to the present chamber configuration. The 832 electronic channels are hosted in two analog/ADC crates and two digital processing crates. A pair of NIM crates are also included for trigger generation, calibration pulser, intermediate voltage power supplies, level meter control and purity monitor.

## 4. The cryostat

The liquid Argon TPC described in section 3 is hosted in a double wall, vacuum insulated and liquid $N_2$ cooled cryostat (see Figure 10). Both the inner and the outer vessels are flanged in the front and in the backsides for easy insertion of the TPC complex. The mechanical construction is designed to be built by stainless steel casting with 5 *mm* wall thickness with proper thickenings for flanges. The inner and outer front flanges have a thin window (0.2 *mm* thick stainless steel) for the beam entrance. Six double wall chimneys are connected, by UHV grade seals, on the topside of the cryostat. Edge welded bellow sections are inserted along their inner tubes as thermal compensators and to make their assembly easy. Two of them are dedicated to the liquid Nitrogen cooling; two are used to empty the inner vessel, filling it by liquid Argon and re-circulating the Argon through outer purifier filters. The last two chimneys are connected to the high voltage feedthrough and to the signal feedthrough.

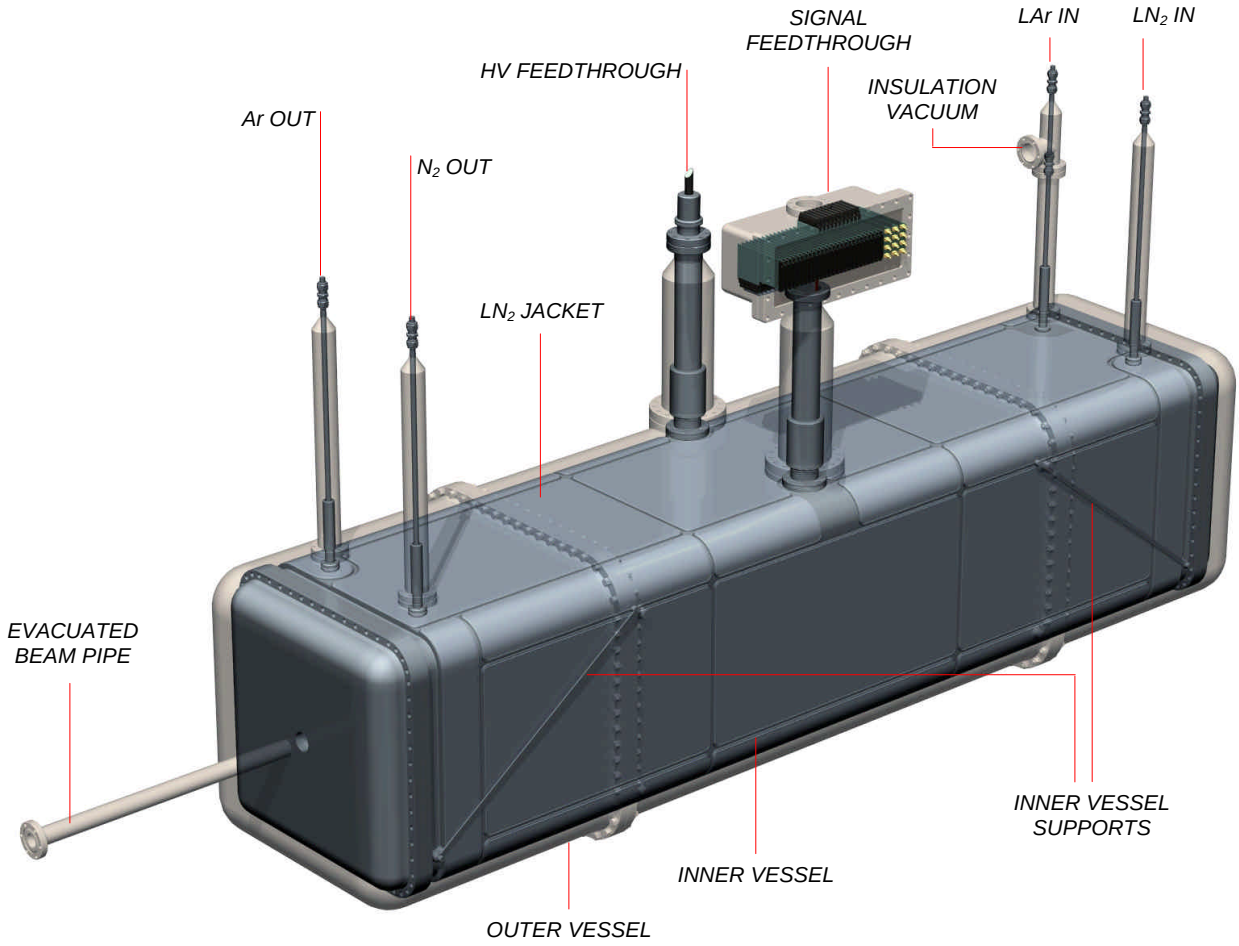


**Figure 10:** The vacuum insulated cryostat.

Four anchor rods, made in invar and linked to the outer vessel, support the inner vessel (total weight = 320 *kg* [inner vessel] + 616 *kg* [liquid Argon] + 90 *kg* [TPC structure] = 1026 *kg*; tensile strength = 84 *MPa*, well under the ultimate tensile strength for invar).

### *4.1. Heat input, insulation and LN2 consumption*

Heat is transmitted from the outer room to the liquid Argon by radiation from the outer to the inner vessel and by conduction through the inner vessel supports and through the signal cables. The heat input is compensated by evaporating liquid nitrogen contained in a jacket surrounding the main body of the inner vessel.

The radiation heat, with an exposed surface of ~ 4.4 $m^2$ and with surface emissivities $\varepsilon_{IN}(90°K) = 0.048$ and $\varepsilon_{OUT}(300°K) = 0.08$ (polished stainless steel surfaces) and 20 superinsulation layers, is ~ 0.7 *watt/m*$^2$ for a total of $W_R = 3.1$ *watt*.

The conduction heat flowing through the four anchor rods (length = 57 *cm* and cross-section = 40 *mm*$^2$) is $W_A = 0.8$ *watt*.

The 832 chamber wires are connected to the front-end electronics via 26 twisted pair flat cables. 68 conductors, each made of 7 copper wires, 102 $\mu m$ in diameter, compose each cable. The total copper cross-section is 1 *cm*$^2$. By considering a cable length of 48 cm between the liquid Argon surface (90°*K*) and the signal feedthrough (300°*K*), with a thermal conduction coefficient for copper $\lambda_{Cu}(90°\div300°K) = 900$ *watt/cm*, the conduction heat through cables is $W_C = 18.8$ watt.

The total heat input is $W_{IN} = W_R + W_A + W_C = \sim 23$ *watt*. With an enthalpy drop $\Delta H_{N_2} = 134$ *joule/cm*$^3$ for the liquid Nitrogen evaporation at 90°*K*, $W_{IN}$ is compensated by evaporating $V_{LN_2} = 0.172$ *cm*$^3$*/s* ≡ 14.8 *litre/day*.

## 5. Cryogenic set-up

The cryogenic circuitry required for operating the liquid Argon TPC is configured to allow for the following operations:

- Vacuum inside the cryostat (inner vessel, $LN_2$ jacket, insulation interspace) and inside the different pipes and transfer lines.
- Cooling the inner vessel by filling and pressurising the $LN_2$ jacket.
- Filling the inner detector vessel with LAr, through purification filters.
- Recirculating the Argon vapour by recondensing it inside the purification filters.
- Emptying the inner vessel by back filling to the LAr storage tank (actually through the purification filters).

The thermodynamic operating conditions are controlled and monitored by level meter(s), temperature and pressure gauges. Actual charge attenuation, due to attachment to electronegative impurities, is monitored by selecting special triggers for ionising track completely crossing the active volume from the cathode to the chamber planes.

## 6. The test beam set-up

The test requires the use of a low energy (<10 *GeV/c*) electron beam, at very low rates (few hundreds of particles per second). Standard plastic scintillator counters for coincidence and veto will be used to enable the event acquisition. A possible configuration for beam momentum analysis with a bending magnet, a pair of gas proportional chambers (upstream and downstream the magnet) and the electron beam under vacuum up to the detector should be foreseen for calorimetric calibration.

## Appendix. Time schedule, cost estimate, collaboration

A detailed time schedule and cost estimate can be made only after a final definition of the construction drawings and after obtaining cost and time estimates from the producers and suppliers. As an approximate approach, we can foresee the following:

Time schedule

- Final constructional plans ..... 2 months
- Estimate requests..... 1 month
- Construction ..... 5 months
- Assembling..... 2 months
- Home laboratory test..... 2 months
- Setting up in the experimental area ..... 1 month
- Final test..... 0.5 month
- Data taking ..... 1.5 months
- Data analysis ..... 2 months

Cost estimates

- Magnet ..... 100 k€
- Magnet power supply..... 50 k€
- Cryostat ..... 50 k€
- TPC ..... 15 k€
- Cryostat details (feedthroughs, …) ..... 15 k€
- Storage dewars ..... 13 k€
- Electronics..... 50 k€
- High voltage power supplies..... 15 k€
- Various accessories and contingency..... 32 k€

Total ..... 340 k€

Besides the INFN, physicist groups of other institutions as UCLA, ETH (Zurich), Hawaii, Princeton and CERN expressed their interest in participating in this project.